pHERV-W envelope protein fuels microglial cell-dependent damage of myelinated axons in multiple sclerosis

David Kremer[a], Joel Gruchot[a], Vivien Weyers[a], Lisa Oldemeier[a], Peter Göttle[a], Luke Healy[b], Jeong Ho Jang[b], Yu Kang T. Xu[b], Christina Volsko[c], Ranjan Dutta[c], Bruce D. Trapp[c], Hervé Perron[d], Hans-Peter Hartung[a], and Patrick Küry[a,1]

[a]Department of Neurology, Medical Faculty, Heinrich Heine University, 40225 Düsseldorf, Germany; [b]Montreal Neurological Institute & Hospital, McGill University, Montreal, QC H4A 3K9, Canada; [c]Department of Neurosciences, Lerner Research Institute, Cleveland Clinic, Cleveland, OH 44195; and [d]GeNeuro, CH-1228 Geneva, Switzerland

Edited by Lawrence Steinman, Stanford University School of Medicine, Stanford, CA, and approved May 29, 2019 (received for review January 23, 2019)

Axonal degeneration is central to clinical disability and disease progression in multiple sclerosis (MS). Myeloid cells such as brain-resident microglia and blood-borne monocytes are thought to be critically involved in this degenerative process. However, the exact underlying mechanisms have still not been clarified. We have previously demonstrated that human endogenous retrovirus type W (HERV-W) negatively affects oligodendroglial precursor cell (OPC) differentiation and remyelination via its envelope protein pathogenic HERV-W (pHERV-W) ENV (formerly MS-associated retrovirus [MSRV]-ENV). In this current study, we investigated whether pHERV-W ENV also plays a role in axonal injury in MS. We found that in MS lesions, pHERV-W ENV is present in myeloid cells associated with axons. Focusing on progressive disease stages, we could then demonstrate that pHERV-W ENV induces a degenerative phenotype in microglial cells, driving them toward a close spatial association with myelinated axons. Moreover, in pHERV-W ENV-stimulated myelinated cocultures, microglia were found to structurally damage myelinated axons. Taken together, our data suggest that pHERV-W ENV-mediated microglial polarization contributes to neurodegeneration in MS. Thus, this analysis provides a neurobiological rationale for a recently completed clinical study in MS patients showing that antibody-mediated neutralization of pHERV-W ENV exerts neuroprotective effects.

multiple sclerosis | axonal degeneration | endogenous retrovirus | myeloid cells | demyelination

As early as 1868, Jean-Martin Charcot described axonal degeneration in multiple sclerosis (MS). However, this histopathological hallmark of the disease was only rediscovered in the late 20th century (1). Even though neurodegeneration is already present in relapsing-remitting (RR) MS, it predominates in later progressive MS stages, leading to severe neurological disability (1–6). Among myeloid cells, microglia that originate from the yolk sac are part of the innate immune system of the central nervous system (CNS) and survey its parenchyma responding to various pathogens (7). However, they are not the only population of myeloid cells that play a role in MS, as blood-borne monocytes invading the brain through a leaky blood–brain barrier (BBB) are present in MS lesions as well (8). In the inflamed MS brain, it is therefore challenging to delineate microglia and invading monocytes (9). In this regard, it remains to be shown whether the recently identified transmembrane protein 119 (TMEM119) might facilitate efforts in this direction (10), since there is evidence that it is exclusively expressed in only a subset of microglial cells (11). In addition, we here investigated predominantly progressive MS cases where the BBB is assumed to be mostly intact, restricting peripheral cell infiltration (12). We therefore focused on the brain-resident myeloid cell population of microglia for our functional in vitro analyses. In MS, microglia participate in both autoimmune inflammation and neurodegeneration by producing proinflammatory cytokines and molecules (4, 13–15). This crucial role is underlined by experiments which found that blocking microglial activation represses the experimental MS model experimental autoimmune encephalomyelitis (16). Microglia also seem to be linked to disease progression in MS: Positron emission tomography (PET) studies in relapsing and progressive MS using the mitochondrial translocator protein TSPO, which is up-regulated in activated microglia, demonstrated that microglial activation is a significant predictor of disability in progressive MS (15, 17). However, microglia can also contribute to neurorepair, *inter alia*, via myelin debris clearance, which is key for remyelination and neuroprotection (18). Therefore, over the years, a distinct nomenclature was established to capture the complex role of this cell population in disease: A phenotype classically categorized as "M1" produces reactive oxygen and nitrogen species, as well as

Significance

There is a broad repertoire of immunomodulatory drugs that effectively treat the inflammatory aspects of relapsing multiple sclerosis (MS). However, axonal degeneration, which occurs mainly in progressive MS, is still not understood and cannot be treated pharmaceutically. As it is the major factor contributing to clinical disability in MS, it represents an unmet clinical need. A recently completed phase IIb study has demonstrated that anti-pathogenic human endogenous retrovirus type W (pHERV-W) envelope protein (ENV) treatment results in a significant decrease of neurodegenerative brain atrophy in treated MS patients. For these results, the work presented here offers an explanation by demonstrating that, via myeloid cells, pHERV-W ENV directly harms axons.

Author contributions: D.K., J.G., H.P., and P.K. designed research; D.K., J.G., V.W., L.O., P.G., L.H., J.H.J., Y.K.T.X., and C.V. performed research; P.G., L.H., C.V., R.D., and B.D.T. contributed new reagents/analytic tools; D.K., J.G., V.W., L.H., J.H.J., Y.K.T.X., R.D., B.D.T., H.P., H.-P.H., and P.K. analyzed data; and D.K. and P.K. wrote the paper.

Conflict of interest statement: J.G., V.W., L.O., L.H., J.H.J., Y.K.T.X., C.V., and R.D. have no competing interests. D.K. received compensation for speaking from Grifols SA. B.D.T. received consultant and speaking fees from Biogen, Genentech, and Sanofi Genzyme. He receives advisory board fees from Disarm Therapeutics and Sanofi Genzyme. He is founder, chair of the Scientific Advisory Board, and chief scientific officer of Renovo Neural. P.G. and P.K. performed consultancy work for GeNeuro. P.K. received compensation for speaking from Sanofi Genzyme. H.P. receives compensation for his work by GeNeuro and is inventor on patents owned by BioMérieux, INSERM, or GeNeuro, but has transferred all his rights to BioMérieux or to GeNeuro under applicable laws for employed inventors. H.-P.H. received compensation for consulting, speaking, and serving on steering committees from Bayer Healthcare, Biogen, GeNeuro, MedImmune, Merck, Novartis, Opexa, Receptos Celgene, Roche, Sanofi Genzyme, and Teva with approval by the rector of Heinrich Heine University.

This article is a PNAS Direct Submission.

See Commentary on page 14791.

[1]To whom correspondence may be addressed. Email: kuery@uni-duesseldorf.de.

Published online June 18, 2019.

proinflammatory cytokines, leading to myelin destruction and subsequent neurodegeneration. In contrast, the so-called "M2" phenotype is associated with the production of antiinflammatory molecules and the clearance of myelin debris (18, 19). However, M1 and M2 states never occur as pure phenotypes in vivo. As a result, while this nomenclature may serve as a tool to simplify data interpretation, this concept remains artificial and is increasingly viewed as insufficient in the field (20). Accordingly, we refrained from using this nomenclature in the work presented here. In this study, we set out to investigate if the envelope protein (pathogenic human endogenous retrovirus type-W [pHERV-W] ENV, formerly MS-associated retrovirus [MSRV]-ENV) of the HERV-W can drive microglia to promote axonal degeneration in MS. HERVs represent 8% of the human genome and originate from mammalian germ-line retroviral infections millions of years ago (21, 22). Usually epigenetically silenced, transactivation by exogenous viral infection such as Epstein–Barr virus or other viruses epidemiologically associated with MS may lead to their (re)expression (23–25). Accordingly, in both clinically isolated syndrome (CIS) and clinically definite (CD) MS, elevated concentrations of pHERV-W ENV protein, RNA, and/or DNA can be found in the serum, cerebrospinal fluid (CSF), and brain (26–28). In addition, pHERV-W positivity is correlated with a more rapid clinical disease progression and increased conversion rate to secondary progressive (SP) MS (29). In previous studies, we demonstrated that the pHERV-W ENV protein interferes with myelin repair by inhibiting oligodendroglial precursor cell (OPC) differentiation via the induction of nitrosative stress through activation of Toll-like receptor 4 (TLR4) (27). This process can be rescued by the humanized anti-ENV IgG_4 monoclonal antibody GNbAC1 (30). In a recently completed phase IIb clinical study, GNbAC1 was shown to exert neuroprotective effects in MS patients (Clinical Trial Assessing the HERV-W pHERV-W ENV Antagonist GNbAC1 for Efficacy in MS [CHANGE-MS]; ClinicalTrials.gov identifier NCT02782858). MRI data demonstrated that anti–pHERV-W ENV treatment results in a significant 31% reduction of cortical atrophy and a 72% reduction of thalamic atrophy. Moreover, GNbAC1 reduced the number of T1 hypointense lesions (so-called "black holes") by 63% within 1 y of treatment. Black holes are considered an MRI correlate of permanent tissue destruction in the brain.

In the study presented here, we found that pHERV-W ENV protein is present on TLR4-positive microglia in MS lesions tightly associated with myelinated axons. In primary microglia, pHERV-W ENV induces ameboid cell morphologies, increases cell proliferation, promotes the secretion of proinflammatory agents, reduces the expression of neuroprotective factors, and diminishes myelin clearance capacity. Furthermore, in ENV protein-stimulated myelinated cocultures, microglia are driven to associate themselves with axons, resulting in the leakage of intraaxonal and myelin proteins. These observations suggest that in the MS brain, pHERV-W ENV may induce myeloid cells to cause damage of myelinated axons. Our work suggests that pHERV-W ENV-mediated modulation of microglial cell polarization fuels and contributes to axonal damage and neurodegeneration in MS. Thereby, this study provides a biomedical rationale for the results of the above-mentioned CHANGE-MS study.

Results

In MS Lesions, pHERV-W ENV Is Present in Myeloid Cells and the Extracellular Space. We studied pHERV-W ENV protein localization in brain tissue sections of 5 MS patients, 2 amyotrophic lateral sclerosis (ALS) patients, and 2 healthy controls (HCs; Table 1) using immunohistological analyses. In a first step, using 3,3′-diaminobenzidine (DAB) staining, we found that pHERV-W ENV-positive cells were absent in HC brains (Fig. 1*B*), while numerous pHERV-W ENV-immunoreactive cells could be detected in chronic and acute active MS lesions (exemplarily shown for primary progressive [PP] MS case MS 36 in Fig. 1 *A*, *C*, *D*, and *E*). pHERV-W ENV-positive cells were found within the lesion parenchyma (Fig. 1 *A* and *E*), but also as part of perivascular cuffs (Fig. 1 *C* and *D*). Anti-major histocompatibility complex class II (MHCII) DAB staining of serial sections confirmed that the majority of pHERV-W ENV-positive cells featured a myeloid phenotype (Fig. 1*F*). To confirm this morphology-based hypothesis, we next performed fluorescent double immunostaining demonstrating that pHERV-W ENV was present in a subpopulation of ionized calcium binding adaptor molecule 1 (Iba1)/MHCII-positive myeloid cells (Fig. 1 *G*–*G*″ and *H*–*H*″). Moreover, abundant extracellular pHERV-W ENV, conceivably from demised immune cells (27), could be found in the lesion parenchyma (Fig. 1 *G*, right lower corner). Furthermore, we found that pHERV-W ENV-positive myeloid cells also expressed the pHERV-W ENV receptor TLR4 (Fig. 1 *I*–*I*″). In contrast, Iba1-positive myeloid cells in ALS brains, which were used as an other neurological disease (OND) control, were pHERV-W ENV-negative (Fig. 1 *J*–*K*′).

In a second step, we studied how pHERV-W ENV-positive myeloid cells associate themselves with proteolipid protein (PLP)-positive myelinated axons, focusing on the edges of chronic and acute active lesions (exemplarily shown for case MS 36 in Fig. 2), where scarce PLP reactivity allows for closer analysis of cell/cell interactions (Fig. 2 *A* and *A*′). Fluorescent double immunostaining of serial sections of the same lesion demonstrated that pHERV-W ENV-positive myeloid cells were in direct contact with PLP-positive axons (Fig. 2 *B*–*D*) and even wrapped around them as revealed by confocal microscopy (Fig. 2 *B*′, merged z-stack and *C* and *D*, single-layer images). Furthermore, pHERV-W ENV-positive cells could be found in direct vicinity to bulb-like axonal structures (Fig. 2*B*″, merged z-stack). Taken together, these data suggested that in the MS brain, pHERV-W ENV modulates myeloid cell behavior,

Table 1. Clinical features of MS and ALS patients whose brain tissue was used for immunohistochemistry

Case designation	MS subtype	Age, y	Sex	Disease duration, y	EDSS	Tissue (no. of lesions analyzed)
MS 25	SPMS	56	M	33	9.5	Chronic active (3)
MS 36	PPMS	63	F	9	7.5	Chronic active (4)
MS 141	SPMS	57	M	13	8	Chronic active (3)
MS 147	RRMS	50	F	31	1	Acute active (4)
MS 150	SPMS	51	F	23	7	Chronic active (3)
MS 100	HC	47	F	n/a	n/a	n/a
MS 61	HC	90	F	n/a	n/a	n/a
ALS 15	OND	61.6	M	3.0	n/a	n/a
ALS 16	OND	63.7	F	2.1	n/a	n/a

F, female; M, male; n/a, not applicable.

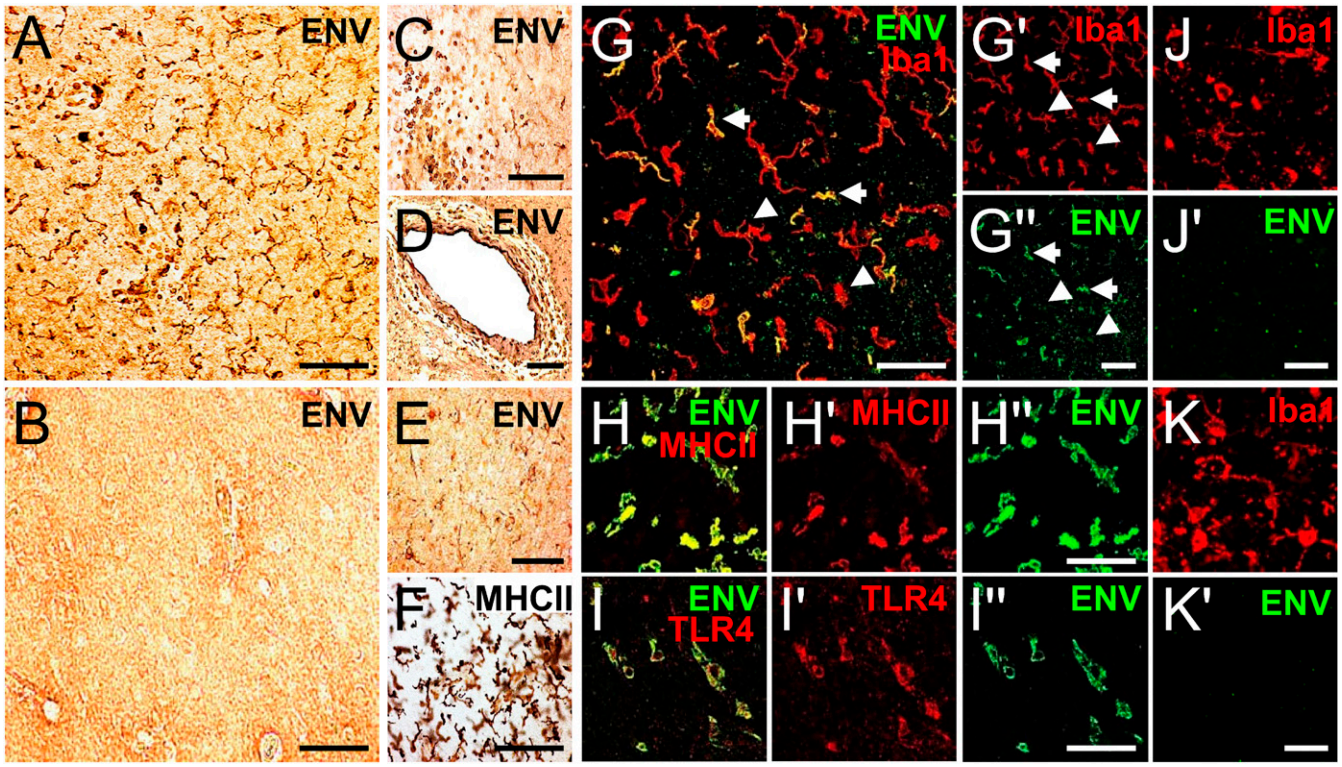

Fig. 1. pHERV-W ENV is present in myeloid cells in MS lesions. (*A* and *C–E*) Anti–pHERV-W ENV DAB staining of an MS lesion (case MS 36) showing pHERV-W ENV-positive cells within the lesion parenchyma (*A* and *E*) and as part of perivascular cuffs (*C* and *D*). (*B*) Control tissue (case MS 100) negative for pHERV-W ENV. A minority of cells feature astrocytic morphologies (*E*), but anti-MHCII DAB staining of a serial section reveals that the majority of pHERV-W ENV-positive cells feature a myeloid phenotype (*F*). (Scale bars: *D*, 80 μm; *A–C*, *E*, and *F*, 50 μm.) (*G–H″*) Double staining demonstrating that pHERV-W ENV (green) is present in a subpopulation of Iba1/MHCII-positive (each in red) myeloid cells in MS lesions (case MS 36). (*G*) Note the extracellular pHERV-W deposits in the right lower corner. Arrows in *G* indicate double-positive cells, and arrowheads point to pHERV-W ENV-negative cells. (Scale bars: *G* and *H″*, 30 μm; *G″*, 50 μm.) (*I–I″*) Double staining demonstrating the expression of pHERV-W ENV receptor TLR4 (red) in pHERV-W ENV-positive cells (green). (Scale bar: *I″*, 30 μm.) (*J–K′*) Double staining demonstrating that pHERV-W ENV (green) is absent in Iba1-positive (red) myeloid cells in ALS tissue (case ALS 15 in *K* and *K′*, case ALS 16 in *J* and *J′*). (Scale bars: *J′* and *K′*, 25 μm.)

driving the myeloid cells toward a physical interaction with axons. Such axon-wrapping myeloid phenotypes were, however, significantly less frequent in Iba1/PLP double-stained ALS tissue sections (Fig. 2 *E–G*).

pHERV-W ENV Induces a Proinflammatory Phenotype in Cultured Microglia. Against the backdrop of the detection of myeloid cell/axon interactions in chronic active lesions of progressive MS cases where the BBB is mostly intact, we used primary rat and human microglial cells for further functional analyses. Immunofluorescent staining of purified CD11b-positive rat microglia confirmed expression of the pHERV-W ENV receptor TLR4 (Fig. 3 *A* and *A′*). Based on previous studies, we stimulated cultured microglia with 1,000 ng/mL recombinant full-length pHERV-W ENV protein for various periods. Note that to confirm the observed effects were ENV- and TLR4-specific, several control experiments have already been performed in previous studies (27, 30, 31). Gene expression analysis revealed a strong induction of proinflammatory markers such as tumor necrosis factor-α (TNF-α), inducible nitric oxide synthase (iNOS), interleukin (IL)-6, and IL-1β (Fig. 3 *B*, *C*, *F*, and *G*). We then corroborated these results using a TNF-α enzyme-linked immunosorbent assay (ELISA) and nitric oxide (NO) spectrometry, respectively, which confirmed increased quantities of TNF-α protein (Fig. 3*D*) and elevated NO levels (Fig. 3*E*) in pHERV-W ENV-stimulated cell culture supernatants. NO and TNF-α are well-established mediators of axonal injury and demyelination (32–35). Further gene expression analysis showed that pHERV-W ENV also reduced the gene expression of triggering receptor expressed on myeloid cells 2 (TREM2; Fig. 4*A*) and protooncogene tyrosine-protein kinase MER (MerTK; Fig. 4*B*), which are key for microglial phagocytosis (36–38). This translated to a functional deficit in myelin uptake capacity in pHERV-W ENV-stimulated microglia as evidenced by diminished in vitro phagocytosis of phRodo-decorated bovine myelin (Fig. 4 *D–F*). As outlined further above, it is known that myelin debris is a major obstacle to neurorepair both as a physicospatial impediment via the expression of axon growth inhibitory molecules and also via an inhibition of OPC differentiation (18, 37–39). In doing so, myelin debris inhibits remyelination (18) so that this microglial core ability has recently become a new target for potential therapeutic approaches (40, 41). Moreover, we observed that pHERV-W ENV stimulation led to a pronounced morphological shift to ameboid microglial phenotypes typical of proinflammatory activation already apparent after 1 and 2 d of pHERV-W ENV stimulation (Fig. 4 *G–I*). In addition, we found that pHERV-W ENV strongly induced microglial proliferation as revealed by Ki-67 expression (Fig. 4*C*).

pHERV-W ENV Treatment Decreases Microglial Expression of Neuroprotective Molecules. In addition to its properties as a proinflammatory agent, we found that stimulation of microglia with pHERV-W ENV protein led to a significant reduction of neuroprotective features as exemplified by gene expression analysis of insulin-like growth factor 1 (IGF-1; Fig. 5*A*), colony stimulating factor 1 (CSF-1; Fig. 5*C*), and fibroblast growth factor 2 (FGF-2; Fig. 5*D*). This also

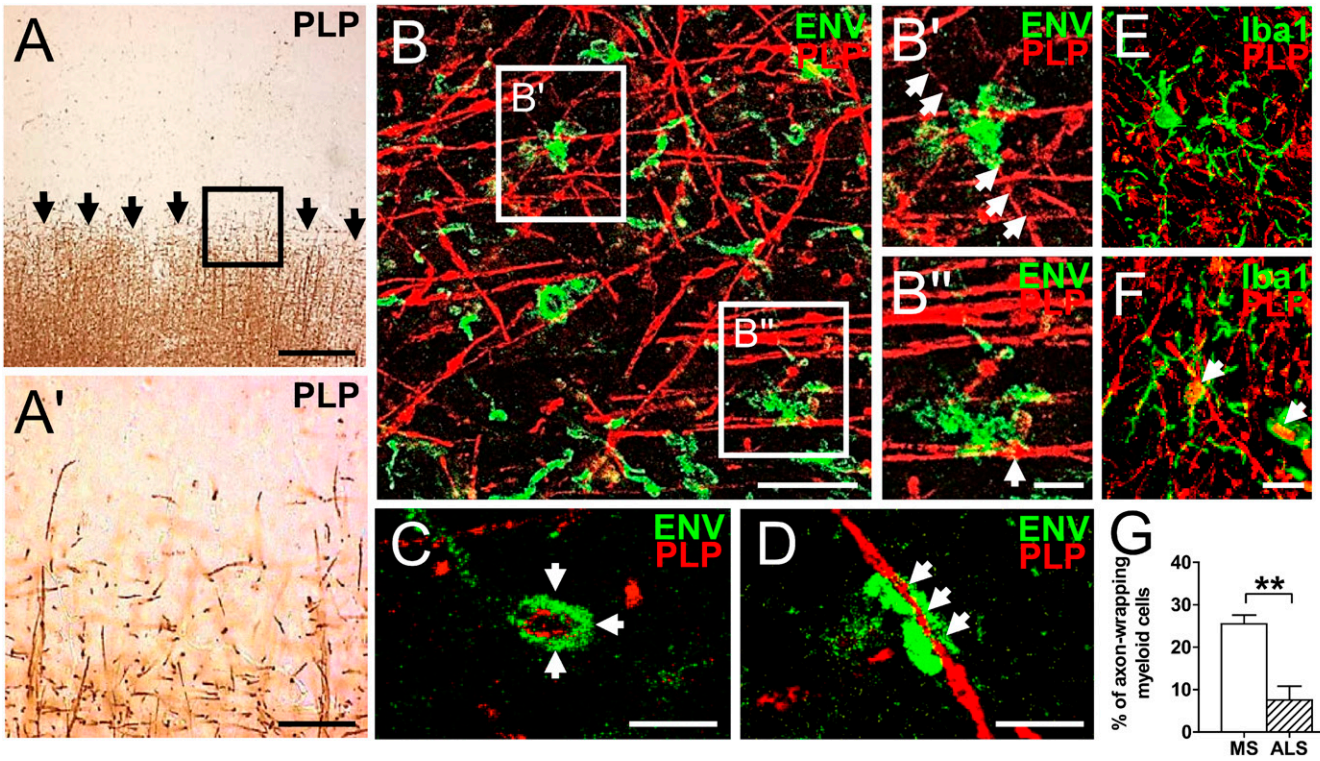

Fig. 2. pHERV-W ENV-positive myeloid cells interact with PLP-positive axons in MS lesions. (*A* and *A′*, *Inset*) Anti-PLP DAB staining of the edge of a chronic active MS lesion (case MS 36). Arrows in *A* indicate the lesion border. (Scale bars: *A*, 200 μm; *A′*, *Inset*, 100 μm.) (*B–B′′*) Double immunostaining (merged z-stack) of serial sections of the same lesion (PLP, red; pHERV-W ENV, green). (*B′* and *B′′*, *Insets*) pHERV-W ENV-positive myeloid cells are in direct contact with PLP-positive axons. Arrows in *B′* point to an axon completely wrapped by pHERV-W ENV-positive myeloid cells. The arrow in *B′′* points to a bulb-like axonal structure indicating damage. (Scale bars: *B*, 30 μm; *B′* and *B′′*, 10 μm.) (*C* and *D*) Single-layer confocal imaging showing that pHERV-W ENV-positive cells completely wrap around PLP-positive axons (arrows). (Scale bars: 20 μm.) Representative photographs of axon-wrapping (*F*) and nonwrapping (*E*) myeloid cells in ALS sections (case ALS 15) are revealed by double immunostaining (Iba1, green; PLP red). (Scale bar: 10 μm.) (*G*) Quantification of myeloid cells with axon-wrapping morphologies in MS and ALS tissue sections. Student's 2-tailed *t* test, unpaired: $^{**}P < 0.01$ ($n = 5$ for MS, $n = 2$ for ALS).

translated to decreased protein levels as exemplarily corroborated by IGF-1 ELISA of cell culture supernatants (Fig. 5*B*). IGF-1 has been described to protect OPCs from cell death (42) and to amplify the positive effects of FGF-2 on OPC proliferation (43). Furthermore, it has been described as a stimulator of myelin synthesis (44). CSF-1, on the other hand, decreases proinflammatory cytokine expression, protects oligodendrocytes from apoptosis (45), and exerts neuroprotective effects on neurons (46).

pHERV-W ENV Protein Induces a Proinflammatory Antiregenerative Phenotype in Human Adult Microglia. To translate our findings to the human paradigm, we investigated the key effects of pHERV-W ENV on purified human adult microglia. As revealed by phalloidin-fluorescein isothiocyanate (FITC) staining, stimulation of these cells with pHERV-W ENV resulted in morphological changes such as elongated and ameboid cell morphologies (Fig. 6 *A* and *B*). This morphological shift was accompanied by increased TNF-α and IL-6 transcript levels (Fig. 6 *C* and *D*), which translated to significantly increased respective protein levels in the culture supernatants (Fig. 6 *G* and *H*). In line with previous observations which have substantiated that iNOS/NO is not easily induced in human myeloid cells (summarized in ref. 47), we found no iNOS expression in human microglial cells following pHERV-W ENV stimulation. In contrast, microglial expression of the phagocytosis-associated genes TREM2 and MerTK was significantly decreased in pHERV-W ENV-stimulated microglia (Fig. 6 *E* and *I*). This was also the case for the neuroprotective growth factors IGF-1 and CSF-1 as demonstrated by gene expression analysis (Fig. 6 *F* and *J*). Taken together, these observations in human adult microglia confirmed the results generated in rodent cells.

pHERV-W ENV Induces a Microglia/Axon Association Resulting in Axonal Injury. Taking into account that no ideal animal model for progressive MS exists, and given the fact that transgenic expression of this particular HERV element is currently not established, we used a primary rat coculture system to study interactions between microglia and myelinated axons. To this end, primary rat microglia were added to myelinated neuron/oligodendrocyte cocultures shortly after the peak of their myelination (Fig. 7*A*). On the following day, pHERV-W ENV protein was added to the medium. As revealed by anti-Iba1 immunostaining, pHERV-W ENV stimulation of microglia-containing cocultures led to a shift of microglial phenotypes (Fig. 7 *B–D′′′′*) similar to the morphological changes observed in rodent and human microglial monocultures (Figs. 4 and 6). Double labeling of myelin basic protein (MBP)-positive myelinated axons and Iba1-positive microglial cells demonstrated a significant increase in activated microglia physically associated with myelinated axons following pHERV-W ENV stimulation throughout the whole observation period (Fig. 7 *E–G′*) providing an in vitro recapitulation of the observations made in MS tissue (Fig. 2). Of note, pHERV-W ENV stimulation did not lead to a reduction of the overall percentage of either Iba1-positive microglia or MBP-positive myelinated axons in comparison to controls (Fig. 7 *E′* and *E′′*). In addition, pHERV-W ENV-stimulated microglia were found to induce neurofilament light chain (NFL), synaptophysin (SYP), and MBP leakage from axons as revealed by ELISA of supernatants from

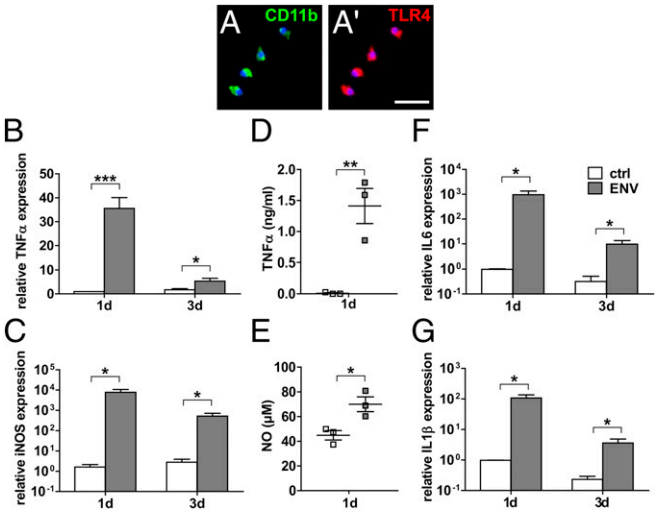

Fig. 3. pHERV-W ENV induces a proinflammatory phenotype in TLR4-positive microglial cells. (*A* and *A′*) TLR4-positive primary rat microglial cells stimulated with pHERV-W ENV protein over a total period of 3 d feature a strong induction of the proinflammatory markers TNF-α (*B*), iNOS (*C*), IL-6 (*F*), and IL-1β (*G*) compared with controls (ctrl). (Scale bar: 20 μm.) Multiple Student's 2-tailed *t* test, unpaired: $*P < 0.05$, $***P < 0{,}001$ ($n = 6$). (*D* and *E*) ELISA-based quantification of TNF-α levels and spectrometry of NO in cell culture supernatants of pHERV-W ENV-stimulated microglia confirms increased levels of these proinflammatory agents after 24 h of pHERV-W ENV stimulation. Student's 2-tailed *t* test, unpaired: $*P < 0.05$, $**P < 0.01$ ($n = 3$). Data are presented as mean ± SEM.

pHERV-W ENV-stimulated cocultures (Fig. 8 *A*, *B*, and *D*). Of note, ENV alone did not lead to such effects, pointing to the key role of microglia. This effect was likely mediated by increased TNF-α concentrations (Fig. 8C).

Discussion

Based on histopathological studies, axonal injury is today widely accepted as a core hallmark of MS (48). Mechanistically, repeated demyelination during the course of MS is thought to lead to the degeneration of axon fibers (49). Accordingly, NFL levels in the CSF of MS patients correlate directly with Expanded Disability Status Scale (EDSS) scores (50), supporting histopathological observations (3). MRI further corroborates the importance of axonal degeneration in MS as gray matter atrophy correlates with disability progression (51). Even though the exact mechanisms underlying axonal degeneration in MS are currently elusive, Wallerian degeneration initiated at lesion sites (52), dysregulation of calcium homeostasis (53), cytotoxic CD8-positive T cells (54), glutamate excitotoxicity (55), and direct NO toxicity (56) are being discussed in this context. As both histological studies and PET-computed tomography (CT) imaging point to the relevance of myeloid cells such as microglia in MS pathology, research has recently focused on their role in axonal degeneration. As a continuation of our previous studies in which we described how pHERV-W ENV inhibits oligodendroglial differentiation (27, 30), in this study, we propose a mechanism by which axonal injury is driven by pHERV-W ENV-activated microglia. While we found that pHERV-W ENV leads to the loss of both myelin and axon integrity, it remains to be demonstrated which of these structures constitutes the primary target of this pathophysiological process. Despite this aspect, we offer a biomedical rationale for the results of the clinical phase IIb CHANGE-MS study (ClinicalTrials.gov identifier NCT02782858) in which anti-pHERV-W ENV (GNbAC1, temelimab) treatment of RRMS patients resulted in significant neuroprotective effects. Among these effects, the 63% reduction in the number of "black holes," an MRI correlate of permanent tissue damage, is particularly striking as, according to PET-CT studies, these structures contain large numbers of microglia. Of note, the primary endpoint of the CHANGE-MS study was the cumulative number of gadolinium-enhancing lesions seen on brain MRI scans after 6 mo (24 wk) of temelimab treatment. This endpoint was not met, and all 48-wk neurodegenerative MRI analyses, including the above-mentioned reduction in the number of "black holes," as well as brain volume and magnetization transfer ratio measurements, were secondary/exploratory. That is why additional studies in a more appropriate population (i.e., nonactive progressive MS patients) at higher doses are currently in a planning stage.

In previous studies, pHERV-W ENV-positive myeloid cells have been reported to be present in MS lesions (27, 28). Going beyond that, we found here that pHERV-W ENV/TLR4–double-positive myeloid cells are abundantly present in MS lesions, where they are tightly associated with myelinated axons at sites of axonal damage. Whether these cells in the MS brain

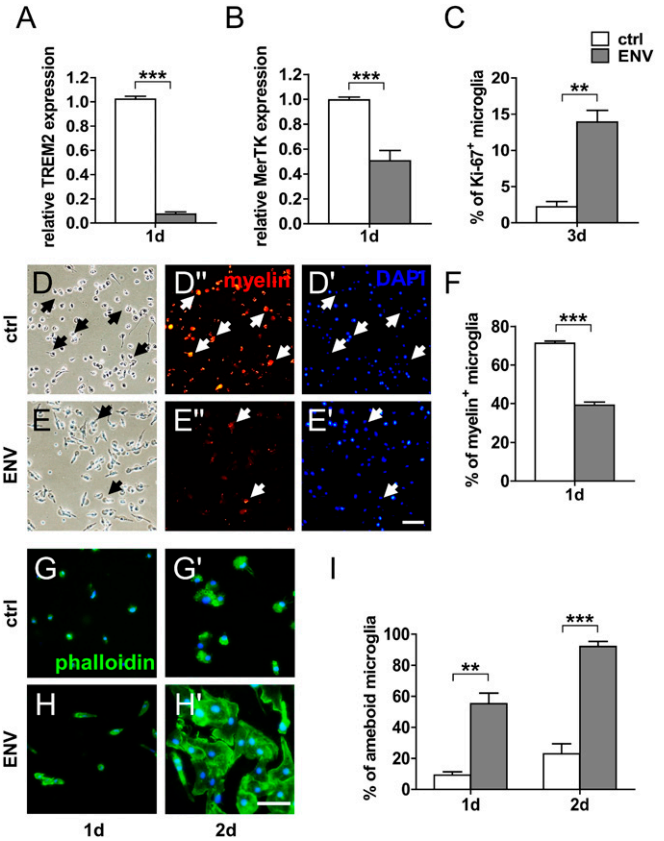

Fig. 4. pHERV-W ENV stimulation decreases the expression of phagocytosis-associated microglial genes, results in diminished myelin phagocytosis capacity, promotes cell proliferation, and induces ameboid microglial morphologies. (*A* and *B*) Gene expression analysis of microglia stimulated with pHERV-W ENV protein shows a significant decrease of the phagocytosis-associated genes TREM2 and MerTK in comparison to controls (ctrl) after 1 d of stimulation. Student's 2-tailed *t* test, unpaired: $***P < 0.001$ ($n = 6$). (*D–F*) Phagocytosis assays with rhodamine-labeled bovine myelin confirm a decreased phagocytosis capacity of microglia stimulated with pHERV-W ENV protein in comparison to ctrl. Arrows indicate rhodamine/myelin-positive cells. Student's 2-tailed *t* test, unpaired: $***P < 0.001$ ($n = 3$). (Scale bar: 40 μm.) (*G–I*) Phalloidin-FITC–based analysis demonstrating that pHERV-W ENV induces an ameboid microglial phenotype already after 1 d of stimulation. Multiple Student's 2-tailed *t* test, unpaired: $**P < 0.01$, $***P < 0.001$ ($n = 3$). (Scale bar: 30 μm.) (*C*) Ki-67–based analysis following 3 d of stimulation reveals that pHERV-W ENV increases microglial proliferation. Student's 2-tailed *t* test, unpaired: $**P < 0.01$ ($n = 3$). Data are presented as mean ± SEM.

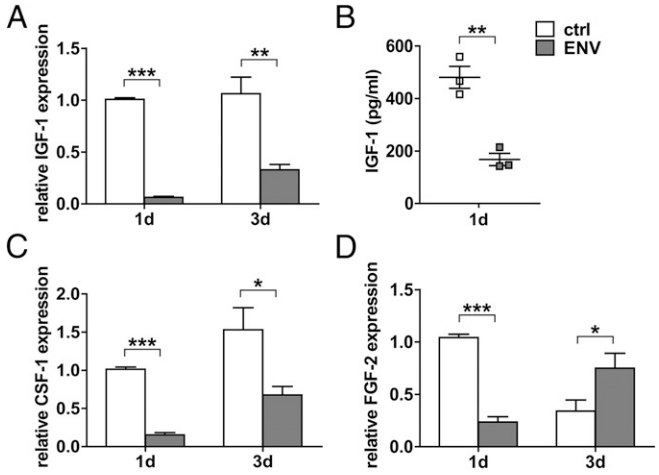

Fig. 5. pHERV-W ENV decreases microglial expression of regenerative factors. Stimulation of microglia with pHERV-W ENV protein results in a significant decrease of the transcription of the regenerative genes IGF-1 (*A*), CSF-1 (*C*), and FGF-2 (*D*) exemplarily confirmed by IGF-1 ELISA showing decreased levels of this protein in cell culture supernatants (*B*). Student's 2-tailed *t* test, unpaired: $*P < 0.05$, $**P < 0.01$, $***P < 0.001$ (*A*, *C*, and *D*, $n = 6$; *B*, $n = 3$). Data are presented as mean ± SEM. ctrl, controls.

express pHERV-W ENV themselves or if they phagocytose extracellular pHERV-W ENV, possibly previously imported into the CNS by other cells, is currently unclear. Mechanistically however, this aspect is probably less important, given the fact that the pHERV-W ENV receptor TLR4 has been described as both a surface and intracellular receptor (57, 58). Of note, TLR4 is also involved in the innate immune response to respiratory syncytial virus through an interaction with the viral envelope fusion protein (59, 60). The decisive finding of this study is that pHERV-W ENV-activated microglia cause a breakdown of both axonal and myelin sheath integrity leading to leakage of intraaxonal and myelin proteins. Mechanistically, this can be explained by our in vitro experiments in both rodent and human microglia demonstrating that pHERV-W ENV induces a cellular phenotype secreting noxious molecules such as TNF-α and NO that are harmful to axons. Furthermore, we could demonstrate that pHERV-W ENV drives microglia to associate themselves with axons in myelinated neuron/oligodendrocyte cocultures in vitro. In this context, the question arises as to whether, in MS, pHERV-W ENV-positive microglia/monocytes are a primary mediator of axonal injury or if they are merely secondarily chemoattracted to axons that are already injured or (partially) demyelinated. However, even if pHERV-W ENV-positive activated cells were only to associate themselves with axons "at risk" secondarily or parallel to occurring damage, they contribute to further axonal demise as we demonstrate here. It therefore remains to be shown whether future MS model systems mimicking pHERV-W reactivation and expression will be able to shed further light on the exact underlying kinetics. Finally, it is intriguing that the CHANGE-MS trial results were obtained in an RRMS population where classically inflammation is assumed to outweigh degeneration. The results of this study therefore underline once more the relevance of neurodegeneration even in early MS. Mirroring this, beyond PPMS and SPMS brains, we also found pHERV-W ENV-positive myeloid cells adjacent to axons in an RRMS brain. Therefore, while future clinical studies will have to assess the effect of anti-ENV treatment in progressive MS, targeting ENV in relapsing subtypes seems to be a worthwhile approach as well.

Materials and Methods

Experimental Design. The primary objective of this study was to establish pHERV-W ENV as a mediator of axonal degeneration in MS. In this regard, we could confirm its presence in myeloid cells in SPMS, PPMS, and RRMS brains by immunohistochemical methods. Functional experiments demonstrating that pHERV-W ENV induces a proinflammatory and antiregenerative microglial phenotype were performed on both rodent and human primary microglia. To clarify the observations made in the MS brain, we used myelinated neuron/glia cocultures to study the interaction between microglia and axons. The number of replicates (*n*) per experiment is noted in each figure legend. The quantitative analyses were performed blinded. One of the limitations of this study consists of the fact that, unfortunately, an animal model featuring transgenic expression of human pHERV-W ENV in microglia is still unavailable. Such a model would have been ideal to study the interaction between pHERV-W ENV-positive microglia and axons in the brain, which, instead, had to be performed in neuron/glia cocultures. In addition, and as a general limitation of most studies in our field, there is no established animal model for progressive MS. A further limitation of this study lies in the fact that it is not a comprehensive retrospective analysis systematically investigating pHERV-W ENV positivity in different MS disease variants and lesion subtypes. For instance, we did not study chronic inactive lesions where the inflammatory process has virtually died out. However, neurodegeneration in these regions has previously been reported to be comparable to levels seen in non-MS control patients (61). Of note, this study was designed as a first neurobiological proof-of-principle approach to establish the basic mechanisms of pHERV-W ENV-induced axonal degeneration. Moreover, a definite distinction between genuine microglia and infiltrating monocytes based on cell surface markers is still challenging despite the recent description of TMEM119, as there is evidence that it is expressed in only a subset of microglial cells.

Immunohistochemistry of Human Tissue Sections. Tissue sections from the brains of 5 MS patients (3 SPMS, 1 PPMS, and 1 RRMS), 2 ALS patients, and 2 HCs were studied (Table 1). All brains were collected as part of the tissue procurement program approved by the Cleveland Clinic Institutional Review Board. All donors or their surrogates gave informed consent for their brains

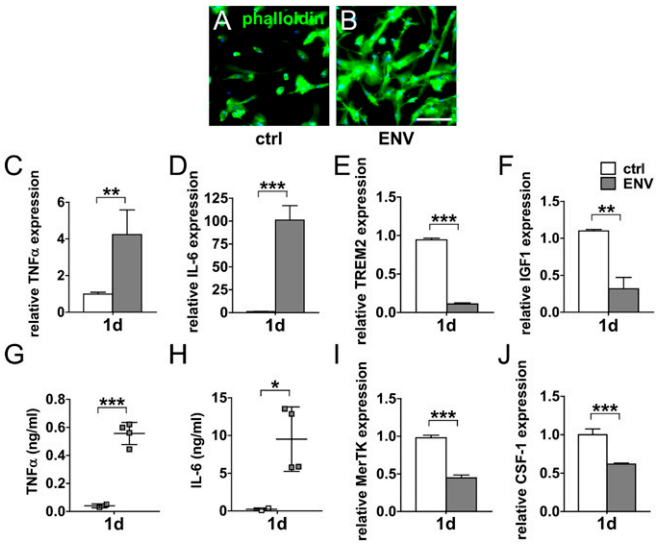

Fig. 6. pHERV-W ENV leads to a proinflammatory antiregenerative phenotype in human adult microglia. (*A* and *B*) Phalloidin-FITC–based analysis of human adult microglia stimulated with pHERV-W ENV protein demonstrating an induction of ameboid phenotypes. (Scale bar: 100 μm.) pHERV-W ENV induces the transcription of proinflammatory genes TNF-α and IL-6 (*C* and *D*), which is mirrored by increased supernatant levels of the respective proteins (*G* and *H*). Student's 2-tailed *t* test, unpaired: $*P < 0.05$, $**P < 0.01$, $***P < 0.001$ ($n = 3$ controls [ctrl], $n = 4$ ENV). (*E* and *I*) pHERV-W ENV stimulation decreases the expression of phagocytosis-associated microglial genes TREM2 and MerTK. (*F* and *J*) pHERV-W ENV also reduces the expression of the regenerative genes IGF-1 and CSF-1. Student's 2-tailed *t* test, unpaired: $**P < 0.01$, $***P < 0.001$ ($n = 3$ ctrl, $n = 4$ ENV). Data are presented as mean ± SEM.

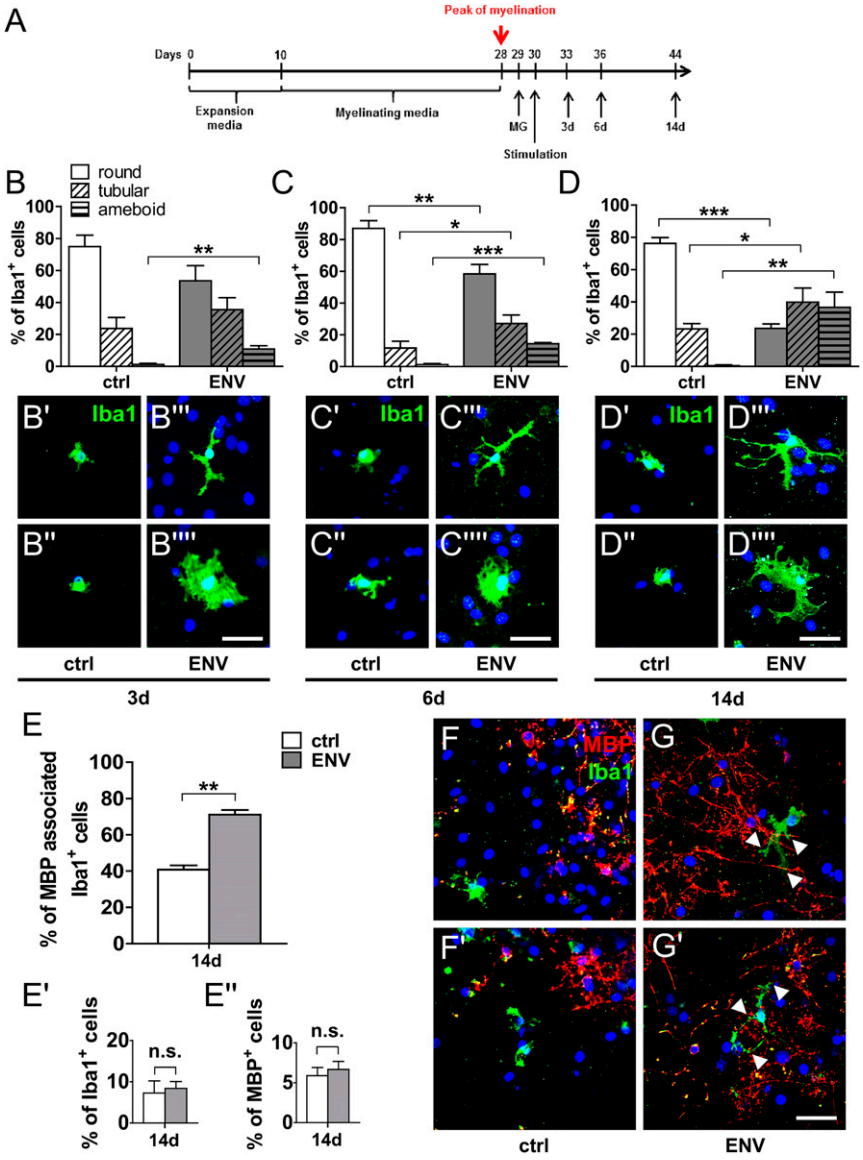

Fig. 7. pHERV-W ENV stimulation induces microglia to associate themselves with myelinated axons. (*A*) Rat primary microglia (MG) were added to neuron/oligodendrocyte cocultures shortly after the peak of myelination, and cultures were stimulated with pHERV-W ENV. (*B–D''''*) Anti-Iba1 immunostaining shows that, mirroring monoculture experiments, pHERV-W ENV leads to a persistent induction of tubular and ameboid microglial phenotypes after as early as 3 d of stimulation in comparison to controls (ctrl). Multiple Student's 2-tailed *t* test, unpaired: $*P < 0.05$, $**P < 0.01$, $***P < 0.001$ ($n = 3$). (*D–D''''*) This effect is sustained over a total period of 14 d. (Scale bars: 50 μm.) (*E–G'*) Double immunostaining of MBP-positive myelinated axons (red) and Iba1-positive microglia (green) in cocultures following 14 d of pHERV-W ENV stimulation demonstrating that pHERV-W ENV leads to a significant increase in microglia associating themselves with axonal structures (arrowheads in *G* and *G'*), mirroring the findings in MS tissue. Student's 2-tailed *t* test, unpaired: $**P < 0.01$ ($n = 3$). n.s., not significant. (Scale bar: 25 μm.) Data are presented as mean ± SEM.

to be used for research studies. All human immunohistochemistry experiments were carried out in accordance with the Cleveland Clinic Institutional regulations and guidelines.

Briefly, MS tissue was fixed in 4% paraformaldehyde (PFA), protected in 70% sucrose, placed on the stage of a sliding microtome, and frozen. Free-floating sections (16–30 μm thick) were cut without exposure to solvents or other embedding mediums. Sections were rinsed in phosphate-buffered saline (PBS) 4 times for 5 min each time, microwaved once for 5 min in 10 mM citrate buffer (pH 6.0), incubated in 3% hydrogen peroxide and 10% Triton X-100 for 30 min, and immunostained by the avidin–biotin complex procedure and with DAB (Sigma–Aldrich) as described previously (62). Sections for confocal fluorescence microscopy were pretreated as described above, incubated with 2 primary antibodies, and then incubated with secondary antibodies (Abcam) conjugated to either Alexa Fluor 594 or Alexa Fluor 488 (Thermo Fisher Scientific). The following primary antibodies were used: mouse anti-MHCII (1/250; Research Resource Identifier [RRID]:AB_2313661; Dako, Agilent Technologies), rat anti-PLP (1/250, hybridoma; a gift from W. Macklin, Department of Cell and Developmental Biology, University of Colorado School of Medicine, Aurora, CO), mouse anti–pHERV-W ENV (GN-mAB_03 [3B2H4], 1/1,000; provided by GeNeuro SA), rabbit anti-TLR4 (1/1,000; RRID:AB_300457; Abcam), and rabbit anti-Iba1 (1/500; RRID:AB_839504; WAKO Pure Chemical Corporation). Anti-ENV/MHCII double staining was carried out sequentially with intermediate blocking and washing steps. Sections were analyzed on a Leica Aristoplan laser scanning microscope (Leitz) and on a Zeiss confocal CLSM 510 microscope. Analysis was performed using ImageJ and Zen 2012 software (Zeiss), respectively. Individual confocal optical sections represented an axial resolution of 0.5 μm. The entire thickness of the section was scanned. Images consisted either of single layers or merged z-stacks combining 16–32 single layers. Fluorescence was collected individually in the green (Alexa 488) and red (Alexa 594) channels to eliminate "bleed-through" from either channel.

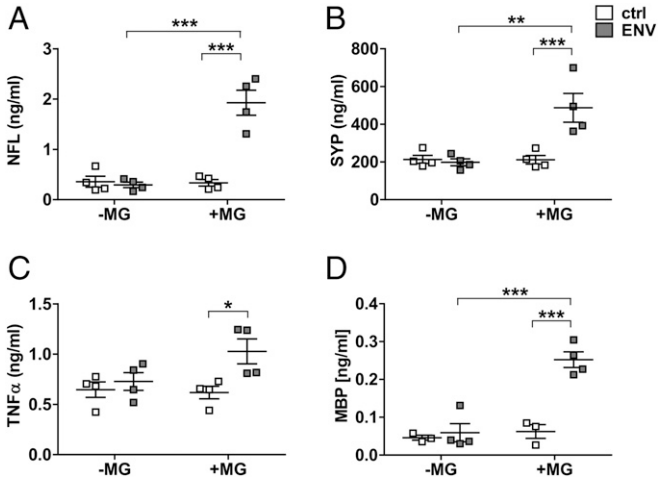

Fig. 8. pHERV-W ENV stimulation induces microglial-dependent injury of myelinated axons. pHERV-W ENV protein-stimulated microglia (MG) induce axonal NFL (*A*), SYP (*B*), and MBP (*D*) leakage as revealed by ELISA of co-culture supernatants. Note that pHERV-W ENV protein and nonstimulated MG alone were unable to exert such effects. (*C*) This was most likely mediated by increased TNF-α levels as revealed by ELISA. Two-way ANOVA, followed by Bonferroni's post hoc test: $*P < 0.05$, $**P < 0.01$, $***P < 0.001$ (n = 3–4). ctrl, controls.

Primary Rat Microglial Cell Culture. All animal procedures were performed in compliance with the experimental guidelines approved by the regional authorities (state agency for Nature, Environment and Consumer Protection of North Rhine Westphalia) and conform to the NIH *Guide for the Care and Use of Laboratory Animals* (63). The Institutional Review Board (IRB) of the ZETT (Zentrale Einrichtung für Tierforschung und wissenschaftliche Tierschutzaufgaben) at the Heinrich Heine University Düsseldorf has approved all animal procedures under licences O69/11 and O82/12. Briefly, dissociated postnatal day 1 (P1) Wistar rat cortices were cultured on poly-D-lysine–coated cell culture flasks in Dulbecco's modified Eagle's medium (DMEM; Thermo Fisher Scientific) substituted with 10% fetal calf serum (FCS; Lonza), 4 mM L-glutamine (Invitrogen), and 50 U/mL penicillin/streptomycin (Invitrogen) as previously described (30, 64–67). After 10 d, flasks were shaken at 180 rpm for 2 h. Microglia-containing supernatants were transferred to bacterial dishes and kept in the incubator, allowing for cell attachment to the surface. Culture flasks were again loaded with fresh DMEM and shaken for another 24 h to increase the final cell yield. Afterward, supernatants were again transferred to bacterial dishes to allow for attachment. Microglia-containing bacterial dishes from the first and second shaking steps were checked for viability via bright-field microscopy, medium was discarded, and cells were rinsed with PBS. Microglia were dislodged by accutase (Thermo Fisher Scientific), which was stopped by FCS-containing DMEM. Microglial cell suspensions were then centrifuged for 5 min at 1,500 rpm at 4 °C. Cell-free supernatants were discarded. Cell pellets were then resuspended in 80 μL of magnetic activated cell sorting (MACS) buffer containing 0.5% bovine serum albumin (BSA) in PBS, and 20 μL of CD11b/c microbeads (Miltenyi Biotec) was added for 15 min at 2–8 °C to allow for binding. Cells were then washed adding 2 mL of MACS buffer and spun down for 5 min at 1,500 rpm at 4 °C. Supernatants were again discarded, and pellets were resuspended in 500 μL of MACS buffer and subjected to MACS sorting according to the manufacturer's protocol (Miltenyi Biotec). The resulting cell suspension was again spun down for 5 min at 1,500 rpm at 4 °C, pellets were resuspended in 1 mL of DMEM, and cell viability and numbers were quantified using trypan blue staining. Average cell purities as assessed by Iba1 positivity were consistently *ca.* 98%. Microglia were seeded on cell culture dishes at different concentrations in DMEM containing 10% FCS and 2 mM L-glutamine.

Microglial Culture Experiments. pHERV-W ENV stimulation of both human and rat primary cells was carried out at a concentration of 1,000 ng/mL recombinant full-length ENV protein with respective buffer volumes as controls as previously described (27, 30). Recombinant ENV protein was produced by Protein'eXpert according to quality control specifications of GeNeuro SA. Endotoxin levels were below the detection limit (<5 endotoxin units [EU]/ml) as measured by the limulus amebocyte lysate test. Control experiments to confirm ENV- and TLR4-specific effects were previously published (27, 30, 31). NO spectrometry and TNF-α and IGF-1 ELISAs of rat microglial cell culture supernatants were performed after 24 h of pHERV-W ENV stimulation using a Nitric Oxide Assay Kit (Merck), a rat TNF alpha ELISA Kit (Abcam), and a Quantikine ELISA Kit (R&D Systems), respectively, according to the manufacturers' protocols. ELISAs of human microglial cell culture supernatants were performed after 24 h of pHERV-W ENV stimulation using a TNF-α ELISA (catalog no. 555212; BD Biosciences), an IL-6 ELISA (catalog no. 555220; BD Biosciences), and an IGF-1 ELISA (catalog no. DY291; R&D Systems) according to the manufacturers' protocols. Immunocytochemistry was performed using previously described protocols (27, 30). Briefly, microglia were fixed with 4% PFA, washed with PBS, blocked for 45 min using 2% normal goat serum (Sigma–Aldrich) and 0.5% Triton X-100 (Sigma–Aldrich) in PBS, and subjected to incubation at 4 °C overnight in 2% normal goat serum (Sigma–Aldrich) and 0.1% Triton X-100 (Sigma–Aldrich) in PBS with mouse anti-CD11b (1/500; RRID:AB_395560; BD Biosciences), mouse anti-TLR4 (1/1,000; RRID:AB_300457; Abcam), and rabbit anti-Ki67 (1/250; RRID:AB_302459; Abcam). Following PBS washes, secondary anti-mouse and anti-rabbit antibodies conjugated with Alexa Fluor 594 (1/500; Thermo Fisher Scientific) were added for 2 h at room temperature. Nuclei were stained with 4′, 6-diamidino-2-phenylindole (DAPI; Roche). Cells were mounted using Citifluor (Citifluor) and analyzed with an Axio Cam HRc microscope (Zeiss). For morphology experiments, microglial F-actin was visualized with FITC-conjugated phalloidin (Sigma–Aldrich) according to the manufacturer's protocol. Myelin phagocytosis experiments were carried out using purified bovine myelin (68) and phRodo (Thermo Fisher Scientific). Briefly, 1 mg of myelin was resuspended in 1 mL of PBS at pH 8. Afterward, 10 μL of phRodo was added and the mix was incubated on a shaker for 1 h at room temperature. The phRodo/myelin was then centrifuged at 1,500 rpm for 10 min. The pellet was resuspended in 1 mL of fresh PBS (pH 8) and diluted to a final concentration of 20 μg/mL. Twenty microliters of phRodo/myelin/PBS was then added to pHERV-W ENV-stimulated and control cells, respectively. Upon a 3-h incubation step at 37 °C, cells were rinsed 3 times with PBS and fixed with 4% PFA. After staining with DAPI, phRodo/myelin-positive microglia were quantified. Images (20× magnification; Zeiss Axionplan 2 microscope) were captured using the same light intensity and filters for all images to be compared and were processed with Axiovision 4.2 software (Zeiss; RRID: SciRes_000111). The analysis was done using Java software (ImageJ, RRID: nif-0000-30,467/ Wright Cell Imaging Facility, RRID:nif-0000-30,471). Immunopositive cells were counted in 9 randomly chosen fields per coverslip. Two coverslips were used per condition. The total number of cells per field was determined via DAPI staining. For quantification, the number of immunopositive cells was compared with the total cell number and expressed as a percentage (mean ± SEM) as previously described (67).

Primary Human Microglial Cell Culture. Adult microglia were derived from surgical resection of brain tissue from pharmacologically intractable non-malignant temporal lobe epilepsy cases, and secondary use of deidentified tissues was approved and carried out in accordance with the guidelines set by the McGill University Institutional Review Board in conjunction with the McGill University Health Centre Ethics Board under protocol ANTJ1989. Tissue provided was outside of the suspected focal site of epilepsy pathology, histopathological changes were excluded by an experienced neuropathologist, and histologically healthy specimens were included. Human microglia were isolated from this adult brain tissue using previously described protocols (69, 70). Briefly, tissue was obtained in pieces <1 mm^3 and treated with DNase (Roche) and trypsin (Thermo Fisher Scientific) for 30 min at 37 °C. Following dissociation through a nylon mesh (37 μm), the cell suspension was separated on a 30% Percoll gradient (GE Healthcare) at 31,000 × g for 30 min. Glial cells (oligodendroglia and microglia) were collected from underneath the myelin layer, washed, and plated at a density of 2×10^6 cells per milliliter in tissue-culture flasks. After 24 h in culture, microglia were separated by the differential adhesion properties of the cells. Microglia were grown for 4 d in flasks before gentle collection using 2 mM ethylenediaminetetraacetic acid (Sigma–Aldrich), and were then plated in minimum essential medium (MEM; Sigma–Aldrich) supplemented with 5% FBS (Wisent), 0.1% penicillin/streptomycin (Thermo Fisher Scientific), and 0.1% L-glutamine (Thermo Fisher Scientific) at a density of 1×10^6 cells per milliliter in a 6-well plate. pHERV-W ENV protein stimulation was carried out as specified for rat microglial cells. For morphology experiments, microglial F-actin was visualized with FITC-conjugated phalloidin (Sigma–Aldrich) according to the manufacturer's protocol. ELISAs of human microglial cell culture supernatants were performed after 24 h of pHERV-W ENV stimulation using TNF-α ELISA (catalog no. 555212; BD Biosciences), IL-6 ELISA (catalog no. 555220; BD Biosciences)

and IGF-1 ELISA (catalog no. DY291; R&D Systems) according to the manufacturers' protocols.

Myelinated Neuron/Glia Cocultures. Dissociated neuron/oligodendrocyte cocultures were obtained from embryonic day 16 Wistar rat cerebral cortices (Wistar rats of either sex) as previously published (67, 71). Cells were plated on 15-mm poly-D-lysine (0.1 mg/mL)–coated coverslips (65,000 cells per coverslip) and kept in myelination medium consisting of N2 and neurobasal medium (Thermo Fisher Scientific) and containing nerve growth factor (NGF) (50 ng/mL) and NT-3 (10 ng/mL) (both from R&D Systems). After 10 d in vitro (DIV10), insulin was removed and the ratio of the insulin-free N2 to neurobasal medium including B27 supplement (Thermo Fisher Scientific) was adjusted to 4:1. This myelination medium was further supplemented with 60 ng/mL tri-iodo-thyronine (Sigma–Aldrich). Final concentrations of individual N2 medium components (DMEM-F12–based, high glucose; Thermo Fisher Scientific) were as follows: insulin (10 μg/mL), transferrin (50 μg/mL), sodium selenite (5.2 ng/mL), hydrocortisone (18 ng/mL), putrescine (16 μg/mL), progesterone (6.3 ng/mL), biotin (10 ng/mL), and *N*-acetyl-L-cysteine (5 μg/mL) (all from Sigma–Aldrich); BSA (0.1%; Roth); and penicillin/streptomycin (50 units/mL; Thermo Fisher Scientific). At DIV30, cultures were supplemented with primary rat microglial cells in the presence or absence of 1,000 ng/mL recombinant pHERV-W ENV protein for another 3, 6, or 14 d. Then, coverslips were washed with PBS, fixed with 4% PFA, and processed for immunofluorescent staining. Media were changed every 72 h. PFA-fixed cocultures were blocked with PBS containing 0.5% Triton X-100 and 2% normal goat serum, and then incubated overnight in 0.1% Triton X-100 and 2% normal goat serum containing the following primary antibodies: rat anti-MBP (1/250; catalog no. MCA409S; Bio-Rad; RRID:AB_325004), rabbit anti-Iba1 (1/500; WAKO Pure Chemical Corporation; RRID:AB_839504), and mouse antineurofilament (1/1,000; catalog no. SMI-312R-500; BioLegend; RRID:AB_2314906). After 24 h, coverslips were washed with PBS and then incubated in PBS for 2 h with secondary antibodies conjugated to Alexa Fluor 488 (1/500; Thermo Fisher Scientific), Alexa Fluor 594 (1/500; Thermo Fisher Scientific), or Alexa Fluor 405 (1/500; Thermo Fisher Scientific). NFL, SYP, MBP, and TNF-α ELISAs were performed on coculture supernatants collected from DIV2 to DIV5 using rat neurofilament light polypeptide (catalog no. EKC39470; Biomatic), rat SYP (catalog no. LS-F22650; LifeSpan BioSciences, Inc.), rat MBP (catalog no. LS-F4093; LifeSpan BioSciences, Inc.), and rat TNF-α (catalog no. ab100785; Abcam) ELISA kits according to the manufacturers' protocols. All images captured on either a Zeiss Axionplan 2 microscope or a Zeiss confocal CLSM 510 microscope (Zeiss) were captured using the same light intensity and filters. Images were processed with Axiovision 4.2 software or Zen 2012 software (Zeiss). Analysis was performed using Java software (ImageJ). Immunopositive cells were counted in 9 randomly chosen fields per coverslip.

RNA Preparation, cDNA Synthesis, and Quantitative RT-PCR. Total RNA purification from cells was performed using the RNeasy procedure (Qiagen). Isolated RNA was reverse-transcribed using a high-capacity cDNA Reverse Transcription Kit (Thermo Fisher Scientific). Quantitative determination of gene expression levels was performed on a 7900HT sequence detection system (Thermo Fisher Scientific) using Power SybrGreen and TaqMan universal master mixes (Thermo Fisher Scientific) as previously described (27, 30). Primer sequences were as follows: rat iNOS (CTC AGC ACA GAG GGC TCA AAG, TGC ACC CAA ACA CCA AGG T), rat TNF-α (AGC CCT GGT ATG AGC CCA TGT A, CCG GAC TCC GTG ATG TCT AAG T), rat IL-6 (GTT GTG CAA TGG CAA TTC TGA, TCT GAC AGT GCA TCA TCG CTG), rat IL-1β (GAA ACA GCA ATG GTC GGG AC, AAG ACA CGG GTT CCA TGG TG), rat TREM2 (CCA AGG AGC CAA TCA GGA AA, GGC CAG GAG GAG AAG AAT GG), rat MerTK (TCT GAC AGA GAC CGC AGT CTT C, TGG ACA CCG TCA GTC CTT TG), rat IGF-1 (AGACGGGCATTGTGGATGA, ACATCTCCAGCCTCCTCAGATC), rat CSF-1(CGA GGT GTC GGA GCA CTG TA, TCA ACT GCT GCA AAA TCT GTA GGT) and rat FGF-2(TGG TAT GTG GCA CTG AAA CGA, CCA GGC CCC GTT TTG G). Detection of human TNF-α, human IL-6, human TREM2, human MerTK, human IGF-1 and human CSF-1 was done using TaqMan probe sets (Thermo Fisher Scientific) Hs00174128_m1, Hs00174131_m1, Hs00219132_m1, Hs01031979_m1, Hs01547656_m1, and Hs00174164_m1, respectively. Relative gene expression levels were determined according to the ΔΔcycle threshold (ΔΔCt) method (Thermo Fisher Scientific). Each sample was measured in quadruplicate; data are shown as mean values ± SEM, and the *t* test was applied to determine statistical significance (Prism 5.0c; GraphPad Software).

ACKNOWLEDGMENTS. We thank Brigida Ziegler and Marion Hendricks for technical assistance and for the preparation and maintenance of myelinated cocultures as well as the preparation of bovine myelin, respectively. Research on myelin repair and HERVs in the P.K. laboratory was supported by the French societies Fondation pour l'Aide à la Recherche sur la Sclérose en Plaques and Association Française Contre les Myopathies, and by GeNeuro. D.K. was funded by the Deutsche Forschungsgemeinschaft (DFG) while carrying out research at the Cleveland Clinic. Research on myelin repair and neuroregeneration has been supported by DFG Grants KU1934/2-1 and KU1934/5-1 (to P.K.) and by the Stifterverband/Novartisstiftung (P.K.) The MS Center at the Department of Neurology at the Medical Faculty of the Heinrich Heine University in Düsseldorf is supported, in part, by the Walter and Ilse Rose Foundation and the James and Elisabeth Cloppenburg, Peek & Cloppenburg Düsseldorf Stiftung. Research in the B.D.T. and R.D. laboratories is supported by NIH Grant RO1-096148 and National Multiple Sclerosis Society (NMSS) Grant RG-5298. The human tissue collection is maintained with the support of NIH Grant R35-NS091683 (to B.D.T.). Research in the L.H. laboratory has been supported by the Montreal Neurological Institute New Investigator Start-up Fund.

1. B. D. Trapp *et al.*, Axonal transection in the lesions of multiple sclerosis. *N. Engl. J. Med.* **338**, 278–285 (1998).
2. C. Bjartmar, B. D. Trapp, Axonal degeneration and progressive neurologic disability in multiple sclerosis. *Neurotox. Res.* **5**, 157–164 (2003).
3. T. Kuhlmann, G. Lingfeld, A. Bitsch, J. Schuchardt, W. Brück, Acute axonal damage in multiple sclerosis is most extensive in early disease stages and decreases over time. *Brain* **125**, 2202–2212 (2002).
4. A. Kutzelnigg *et al.*, Cortical demyelination and diffuse white matter injury in multiple sclerosis. *Brain* **128**, 2705–2712 (2005).
5. J. W. Peterson, L. Bö, S. Mörk, A. Chang, B. D. Trapp, Transected neurites, apoptotic neurons, and reduced inflammation in cortical multiple sclerosis lesions. *Ann. Neurol.* **50**, 389–400 (2001).
6. K. A. Nave, B. D. Trapp, Axon-glial signaling and the glial support of axon function. *Annu. Rev. Neurosci.* **31**, 535–561 (2008).
7. F. Ginhoux, M. Prinz, Origin of microglia: Current concepts and past controversies. *Cold Spring Harb. Perspect. Biol.* **7**, a020537 (2015).
8. M. Kouwenhoven, N. Teleshova, V. Ozenci, R. Press, H. Link, Monocytes in multiple sclerosis: Phenotype and cytokine profile. *J. Neuroimmunol.* **112**, 197–205 (2001).
9. M. Greter, I. Lelios, A. L. Croxford, Microglia versus myeloid cell nomenclature during brain inflammation. *Front. Immunol.* **6**, 249 (2015).
10. M. L. Bennett *et al.*, New tools for studying microglia in the mouse and human CNS. *Proc. Natl. Acad. Sci. U.S.A.* **113**, E1738–E1746 (2016).
11. J. Satoh *et al.*, TMEM119 marks a subset of microglia in the human brain. *Neuropathology* **36**, 39–49 (2016).
12. J. Correale, M. I. Gaitán, M. C. Ysrraelit, M. P. Fiol, Progressive multiple sclerosis: From pathogenic mechanisms to treatment. *Brain* **140**, 527–546 (2017).
13. C. S. Jack *et al.*, TLR signaling tailors innate immune responses in human microglia and astrocytes. *J. Immunol.* **175**, 4320–4330 (2005).
14. H. Lassmann, Mechanisms of white matter damage in multiple sclerosis. *Glia* **62**, 1816–1830 (2014).
15. P. Giannetti *et al.*, Microglia activation in multiple sclerosis black holes predicts outcome in progressive patients: An in vivo [(11)C](R)-PK11195-PET pilot study. *Neurobiol. Dis.* **65**, 203–210 (2014).
16. F. L. Heppner *et al.*, Experimental autoimmune encephalomyelitis repressed by microglial paralysis. *Nat. Med.* **11**, 146–152 (2005).
17. L. Airas, M. Nylund, E. Rissanen, Evaluation of microglial activation in multiple sclerosis patients using positron emission tomography. *Front. Neurol.* **9**, 181 (2018).
18. A. Lampron *et al.*, Inefficient clearance of myelin debris by microglia impairs remyelinating processes. *J. Exp. Med.* **212**, 481–495 (2015).
19. R. Orihuela, C. A. McPherson, G. J. Harry, Microglial M1/M2 polarization and metabolic states. *Br. J. Pharmacol.* **173**, 649–665 (2016).
20. R. M. Ransohoff, A polarizing question: Do M1 and M2 microglia exist? *Nat. Neurosci.* **19**, 987–991 (2016).
21. C. Feschotte, C. Gilbert, Endogenous viruses: Insights into viral evolution and impact on host biology. *Nat. Rev. Genet.* **13**, 283–296 (2012).
22. P. Küry *et al.*, Human endogenous retroviruses in neurological diseases. *Trends Mol. Med.* **24**, 379–394 (2018).
23. H. Perron *et al.*, Endogenous retroviral genes, herpesviruses and gender in multiple sclerosis. *J. Neurol. Sci.* **286**, 65–72 (2009).
24. F. C. Hsiao *et al.*, EBV LMP-2A employs a novel mechanism to transactivate the HERV-K18 superantigen through its ITAM. *Virology* **385**, 261–266 (2009).
25. C. Nellåker *et al.*, Transactivation of elements in the human endogenous retrovirus W family by viral infection. *Retrovirology* **3**, 44 (2006).
26. H. Perron *et al.*, Human endogenous retrovirus type W envelope expression in blood and brain cells provides new insights into multiple sclerosis disease. *Mult. Scler.* **18**, 1721–1736 (2012).
27. D. Kremer *et al.*, Human endogenous retrovirus type W envelope protein inhibits oligodendroglial precursor cell differentiation. *Ann. Neurol.* **74**, 721–732 (2013).
28. J. van Horssen, S. van der Pol, P. Nijland, S. Amor, H. Perron, Human endogenous retrovirus W in brain lesions: Rationale for targeted therapy in multiple sclerosis. *Mult. Scler. Relat. Disord.* **8**, 11–18 (2016).
29. S. Sotgiu *et al.*, Multiple sclerosis-associated retrovirus and progressive disability of multiple sclerosis. *Mult. Scler.* **16**, 1248–1251 (2010).
30. D. Kremer *et al.*, The neutralizing antibody GNbAC1 abrogates HERV-W envelope protein-mediated oligodendroglial maturation blockade. *Mult. Scler.* **21**, 1200–1203 (2015).

31. A. Rolland *et al.*, The envelope protein of a human endogenous retrovirus-W family activates innate immunity through CD14/TLR4 and promotes Th1-like responses. *J. Immunol.* **176**, 7636–7644 (2006).
32. T. Touil, M. S. Deloire-Grassin, C. Vital, K. G. Petry, B. Brochet, In vivo damage of CNS myelin and axons induced by peroxynitrite. *Neuroreport* **12**, 3637–3644 (2001).
33. M. Karamita *et al.*, Therapeutic inhibition of soluble brain TNF promotes remyelination by increasing myelin phagocytosis by microglia. *JCI Insight* **2**, 87455 (2017).
34. M. S. Petrovich *et al.*, Pentoxifylline suppression of TNF-alpha mediated axonal degeneration in the rabbit optic nerve. *Neurol. Res.* **19**, 551–554 (1997).
35. Y. Kitaoka *et al.*, TNF-alpha-induced optic nerve degeneration and nuclear factor-kappaB p65. *Invest. Ophthalmol. Vis. Sci.* **47**, 1448–1457 (2006).
36. T. K. Ulland, M. Colonna, TREM2–A key player in microglial biology and Alzheimer disease. *Nat. Rev. Neurol.* **14**, 667–675 (2018).
37. L. M. Healy *et al.*, MerTK-mediated regulation of myelin phagocytosis by macrophages generated from patients with MS. *Neurol. Neuroimmunol. Neuroinflamm.* **4**, e402 (2017).
38. L. M. Healy *et al.*, MerTK is a functional regulator of myelin phagocytosis by human myeloid cells. *J. Immunol.* **196**, 3375–3384 (2016).
39. W. F. Blakemore, Regeneration and repair in multiple sclerosis: The view of experimental pathology. *J. Neurol. Sci.* **265**, 1–4 (2008).
40. M. S. Natrajan *et al.*, Retinoid X receptor activation reverses age-related deficiencies in myelin debris phagocytosis and remyelination. *Brain* **138**, 3581–3597 (2015).
41. M. S. Natrajan *et al.*, Pioglitazone regulates myelin phagocytosis and multiple sclerosis monocytes. *Ann. Clin. Transl. Neurol.* **2**, 1071–1084 (2015).
42. S. Lin *et al.*, IGF-1 protects oligodendrocyte progenitor cells and improves neurological functions following cerebral hypoxia-ischemia in the neonatal rat. *Brain Res.* **1063**, 15–26 (2005).
43. F. Jiang, T. J. Frederick, T. L. Wood, IGF-I synergizes with FGF-2 to stimulate oligodendrocyte progenitor entry into the cell cycle. *Dev. Biol.* **232**, 414–423 (2001).
44. R. L. Mozell, F. A. McMorris, Insulin-like growth factor I stimulates oligodendrocyte development and myelination in rat brain aggregate cultures. *J. Neurosci. Res.* **30**, 382–390 (1991).
45. R. Kadota *et al.*, Granulocyte colony-stimulating factor (G-CSF) protects oligodendrocyte and promotes hindlimb functional recovery after spinal cord injury in rats. *PLoS One* **7**, e50391 (2012).
46. J. Luo *et al.*, Colony-stimulating factor 1 receptor (CSF1R) signaling in injured neurons facilitates protection and survival. *J. Exp. Med.* **210**, 157–172 (2013).
47. A. M. Smith, M. Dragunow, The human side of microglia. *Trends Neurosci.* **37**, 125–135 (2014).
48. H. Lassmann, J. van Horssen, The molecular basis of neurodegeneration in multiple sclerosis. *FEBS Lett.* **585**, 3715–3723 (2011).
49. Y. You *et al.*, Demyelination precedes axonal loss in the transneuronal spread of human neurodegenerative disease. *Brain* **142**, 426–442 (2019).
50. C. Malmeström, S. Haghighi, L. Rosengren, O. Andersen, J. Lycke, Neurofilament light protein and glial fibrillary acidic protein as biological markers in MS. *Neurology* **61**, 1720–1725 (2003).
51. C. Jacobsen *et al.*, Brain atrophy and disability progression in multiple sclerosis patients: A 10-year follow-up study. *J. Neurol. Neurosurg. Psychiatry* **85**, 1109–1115 (2014).
52. T. Dziedzic *et al.*, Wallerian degeneration: A major component of early axonal pathology in multiple sclerosis. *Brain Pathol.* **20**, 976–985 (2010).
53. A. Nicot, P. V. Ratnakar, Y. Ron, C. C. Chen, S. Elkabes, Regulation of gene expression in experimental autoimmune encephalomyelitis indicates early neuronal dysfunction. *Brain* **126**, 398–412 (2003).
54. H. Neumann, I. M. Medana, J. Bauer, H. Lassmann, Cytotoxic T lymphocytes in autoimmune and degenerative CNS diseases. *Trends Neurosci.* **25**, 313–319 (2002).
55. M. Kostic, N. Zivkovic, I. Stojanovic, Multiple sclerosis and glutamate excitotoxicity. *Rev. Neurosci.* **24**, 71–88 (2013).
56. K. J. Smith, R. Kapoor, S. M. Hall, M. Davies, Electrically active axons degenerate when exposed to nitric oxide. *Ann. Neurol.* **49**, 470–476 (2001).
57. S. Dunzendorfer, H. K. Lee, K. Soldau, P. S. Tobias, Toll-like receptor 4 functions intracellularly in human coronary artery endothelial cells: Roles of LBP and sCD14 in mediating LPS responses. *FASEB J.* **18**, 1117–1119 (2004).
58. T. Shibata *et al.*, Intracellular TLR4/MD-2 in macrophages senses Gram-negative bacteria and induces a unique set of LPS-dependent genes. *Int. Immunol.* **23**, 503–510 (2011).
59. L. M. Haynes *et al.*, Involvement of toll-like receptor 4 in innate immunity to respiratory syncytial virus. *J. Virol.* **75**, 10730–10737 (2001).
60. E. A. Kurt-Jones *et al.*, Pattern recognition receptors TLR4 and CD14 mediate response to respiratory syncytial virus. *Nat. Immunol.* **1**, 398–401 (2000).
61. B. F. Popescu, I. Pirko, C. F. Lucchinetti, Pathology of multiple sclerosis: Where do we stand? *Continuum (Minneap Minn)* **19**, 901–921 (2013).
62. L. Bö *et al.*, Detection of MHC class II-antigens on macrophages and microglia, but not on astrocytes and endothelia in active multiple sclerosis lesions. *J. Neuroimmunol.* **51**, 135–146 (1994).
63. National Research Council, *Guide for the Care and Use of Laboratory Animals* (National Academies Press, Washington, DC, ed. 8, 2011).
64. D. Kremer *et al.*, p57kip2 is dynamically regulated in experimental autoimmune encephalomyelitis and interferes with oligodendroglial maturation. *Proc. Natl. Acad. Sci. U.S.A.* **106**, 9087–9092 (2009).
65. K. D. McCarthy, J. de Vellis, Preparation of separate astroglial and oligodendroglial cell cultures from rat cerebral tissue. *J. Cell Biol.* **85**, 890–902 (1980).
66. P. Göttle *et al.*, Activation of CXCR7 receptor promotes oligodendroglial cell maturation. *Ann. Neurol.* **68**, 915–924 (2010).
67. P. Göttle *et al.*, Rescuing the negative impact of human endogenous retrovirus envelope protein on oligodendroglial differentiation and myelination. *Glia* **67**, 160–170 (2019).
68. S. W. Brostoff *et al.*, The P2 protein of bovine root myelin: Isolation and some clinical and immunological properties. *J. Neurochem.* **23**, 1037–1043 (1974).
69. B. A. Durafourt, C. S. Moore, M. Blain, J. P. Antel, Isolating, culturing, and polarizing primary human adult and fetal microglia. *Methods Mol. Biol.* **1041**, 199–211 (2013).
70. A. D. Greenhalgh *et al.*, Peripherally derived macrophages modulate microglial function to reduce inflammation after CNS injury. *PLoS Biol.* **16**, e2005264 (2018).
71. P. Göttle *et al.*, Oligodendroglial maturation is dependent on intracellular protein shuttling. *J. Neurosci.* **35**, 906–919 (2015).